Kinetic Monte Carlo simulation of heterogeneous and homogeneous radio-oxidation of a polymer

B. Gervais, Y. Ngono, E. Balanzat

Version of Record: https://www.sciencedirect.com/science/article/pii/S0141391021000136
Manuscript_3ce2b9c69cd27bf340a65d95408b2f2f

Kinetic Monte Carlo simulation of heterogeneous and homogeneous radio-oxidation of a polymer

B. Gervais[1a], Y. Ngono[a], E. Balanzat[a]

[a]*Normandie Univ, ENSICAEN, UNICAEN, CEA, CNRS, CIMAP,UMR 6252, BP 5133 F-14070 Caen Cedex 05 France*

Abstract

Ion irradiation is known to generate well-localized cylindrical ionization and excitation tracks in materials. The resulting radiation chemistry in organic material is thus initiated by a strongly heterogeneous source of radicals. We present a comparison of heterogeneous and homogeneous radio-oxidation kinetics of a polymer. Our analysis is based on a kinetic Monte Carlo simulation of the diffusion-reaction process of radicals in the material. We consider, as a numerical test case, the radio-oxidation of polyethylene by 5 MeV He ions. For heterogeneous kinetics, we show that the spatial distribution of radicals reached in the stationary regime is not homogeneous at the sub-micrometer scale. Both kinetics are quite comparable regarding the variation of the radical concentration with the irradiation time. However, the yield of peroxy radicals reached in stationary regime is significantly lower in the case of heterogeneous kinetics. Moreover, the propagation kinetics characterized by the ratio of POOH over POOP products exhibits very different behaviors with respect to oxygen concentration.

Keywords: theory and modeling, ageing, kinetics, radiation

[1]corresponding author: gervais@ganil.fr

1. Introduction

Radiation-induced modifications in polymers, and more broadly in organic matter, are deeply ruled by the presence, or not, of molecular oxygen dissolved in the polymer. Actually, in most practical cases, polymers are submitted to radiation in air, and under experimental conditions allowing an in-depth oxygen nourishing of the polymer. This induces the so called radio-oxidative ageing. This ageing has been largely studied, not only because of its basic-science interest but also in the sphere of the nuclear power industry, because it induces a degradation of the functional properties of materials. It is then essential to control and predict these changes to avoid unacceptable failures [1]. When used in the nuclear power industry, polymers could be submitted to beta, gamma and alpha radiation.

The standards of the radio-oxidation modelling were proposed, around seventy years ago (1946) by Bolland [2]. Oxidation proceeds via a radical chemistry kinetics that includes a chain reaction (propagation) which is mainly limited by bimolecular terminations. It is interesting to recall that thermo- or photo- oxidative ageing of polymers are essentially governed by very similar kinetics but differ mainly by the initiation step. In several practical cases, radio- and thermal-oxidation occurs simultaneously and both have to be coherently considered in the kinetics [3].

The most stringent consequence of the existence of a chain reaction is that oxidation is not only dose dependent but also dose rate dependent. This dose rate effect is crucial when considering accelerated ageing methods for predicting long-term performance of polymers. Going beyond a phenomenological approach of dose rate effects implies developing a realistic modelling and simulation of the radio-oxidation kinetics.

Several models of chemical kinetics for radio- or radio-thermal-oxidation of polymers have been proposed. Their level of complexity varies as they include more functional groups of the polymer, more additives, more molecular and radical species and chemical reactions. Assuming overall homogeneity and the set-up of a stationary state for the radical concentrations, these models can be translated into a set of coupled differential equations, which is solved numerically [4, 5]. Analytical solutions only exist for some very simplified cases [6]. By far, the reaction rate constants of individual reactions are not well established, neither theoretically nor by very direct experimental determination. Nevertheless a large body of experimental results concerning oxidation is available at different levels: molecular (yields of oxygen uptake, gas release, unsaturated group creation or destruction, oxidized chemical groups like carbonyls, alcohols, acids, hydroperoxides, peroxides etc.); macromolecular (reticulation, chain scission, molecular mass distribution); and macroscopic (for instance mechanical properties). An important work of multiparametric fit of the chemical kinetic model predictions to these experimental data gave some sets of reaction rate constants [5].

It was often recognized that real case of radio-oxidation of polymers has to consider the complexity of "rapid spur reactions involving high concentrations of radicals, and slower reactions of radical escapees, which occur at much lower overall radical concentrations" [7]. However, this was not fully transcribed in the modelling of radio-oxidation performed so far. Because of its unique spatio-temporal structure, the heterogeneity of the energy deposition by radiations, *i.e.* of the initiation step, is in nature very different from spatial heterogeneities [8]

that could exist, for instance, at interfaces between different physical phases or from the spatial heterogeneities of sites at the origin of thermal initiation. We shall refer to the microscopic variation of concentration related to the energy deposition by radiation as heterogeneity though it is sometimes referred to as non-homogeneity [8]. In radio-oxidation of polymers, the macroscopic heterogeneity corresponding to the presence of an O_2 concentration gradient in depth, was extensively studied [9]. Observable effects occur when, for a given sample thickness and O_2 permeation value, the dose rate exceeds a critical value.

By way of comparison, the modelling and simulation of water radiolysis are much better developed than those of polymers are. In the former case, the corpus of experimental data has no common measure with the polymer case. In particular, time-resolved experiments (in the sub-ps - μs range) are possible and widely performed for water. Moreover, the determination of the reaction rate constants of individual reactions in liquids is facilitated by the easy use of scavengers and it is thus easier in liquids than it is in solids. Because of that, the time evolution of all radicals and stable molecules created in the wake of a single projectile was successfully simulated for different irradiation projectiles with very different Linear Energy Transfer (LET) [10, 11, 12], electrons, protons, alpha and heavy ions. However, even for water radiolysis, the long-time evolution and the establishment of steady states, which results from the progressive overlap of tracks generated by different projectiles due to the diffusion of radicals and stable molecules out of each single track, is simply performed by ad-hoc homogenization extrapolated from the so-called primary yields obtained for a single projectile track after 1 μs evolution [13]. Finally, despite evident similarities, heterogeneous kinetics in liquids and solids could be very different because of differences by orders of magnitude in the diffusion coefficient values. To our best knowledge, the radiation-induced heterogeneous kinetics for interacting projectile tracks was not yet formally addressed, with likely the sole exception of the work of V. L. Klochikhin and L. I. Trakhtenberg who consider the simplest case of a bimolecular recombination of radicals [14].

We are interested here in the intrinsic microscopic heterogeneity of radical generation by irradiation. An obvious and practical example of such heterogeneity is the one induced by swift ion irradiation. Such ions release their energy as cylindrical tracks of ionization and excitation, which, after electron-hole pair recombination and bond breaking, turns into tracks of radicals with a few nanometres radial extension. In the present paper, we investigate the difference between the kinetics induced by such a heterogeneous source of radicals and an ideally-homogeneous source, generally considered when studying the radio-oxidation process. We shall considered here a simple generic model presented in section 2, which does not intend to take into account the specificity of a given polymer but rather allows us to distinguish the peculiarities of a heterogeneous source of radicals. A proper account of diffusion reaction process requires the use of a Kinetic Monte Carlo (KMC) simulation, presented in section 3. The results are presented in section 4, where we put some emphasis on the role of O_2 concentration c_{O_2} and dose rate $\dot{D}$, which are the two most obvious parameters controlling the radio-oxidation kinetics, for a given polymer formulation.

2. Model

2.1. Chemical equations

As we wish to focus specifically on the role of heterogeneous generation of radicals by radiation, and to be in position to discuss our result with those obtained by other authors, we follow the rather standard model proposed in the literature [2, 15, 16, 6, 4, 5] for homogeneous kinetics. According to this model, the radiation generates ionization and excitation leading to C-H bond dissociation and to the formation of $P^\bullet$ and $H^\bullet$ radicals. We assume that the liberated $H^\bullet$ radicals leads to fast abstraction of another H atom to form one H_2 and two $P^\bullet$ radicals at the end of the initiation stage. The kinetics of this very short stage is not investigated here, and the possible specific position correlation of the two geminated $P^\bullet$ radicals is neither considered.

Once the $P^\bullet$ radicals are formed along the projectile track, the diffusion-reaction kinetics starts and the formation of products is given by the following system of chemical reactions:

$$\begin{aligned}
P^\bullet + O_2 &\longrightarrow POO^\bullet \\
POO^\bullet + PH &\longrightarrow POOH + P^\bullet \\
P^\bullet + P^\bullet &\longrightarrow P_2 \\
P^\bullet + POO^\bullet &\longrightarrow POOP \\
POO^\bullet + POO^\bullet &\longrightarrow POOP + O_2
\end{aligned}$$

The products POOH, POOP and P_2 are considered non-reactive stable species. In the present study we shall not distinguish between the POOP formed by the reaction $P^\bullet + POO^\bullet \longrightarrow POOP$ from those formed by the reaction $POO^\bullet + POO^\bullet \longrightarrow POOP + O_2$. Moreover, we do not distinguish between the different termination products like acids, ketones, etc ..., as in our simplified scheme POOP represents all the possibilities.

We consider only thin slabs of polymer, so that the O_2 concentration do not vary with time. It is assumed to be at equilibrium with the external atmosphere and it can be monitored by varying the pressure as done experimentally.

The reaction of $POO^\bullet$ with the polymer has been critically discussed in the literature [17] because the hydrogen abstraction is energetically very unfavourable. This reaction should be considered an effective reaction involving potentially a more complex sequence of chemical reactions with several intermediates. Alternative reactions might also be considered. For example, the three-body reaction $POO^\bullet + O_2 + PH \longrightarrow POOH + POO^\bullet$ might take place. At sufficiently high oxygen concentration, it is not conceptually strongly different from the above reactions as it summarizes the second and first equations in one single reaction step. In such a case, the POOH concentration would increase with the time proportionally to the product of the $POO^\bullet$ and O_2 concentrations. Thus, the amount of POOH would vary proportionally to the O_2 concentration when the $POO^\bullet$ concentration saturates. It might be worth investigating such a variation experimentally to clarify the nature of the propagation reaction.

The model considered here is of course an ideal case for very long polyethylene chains. We do not consider other specific polymers in their whole complexity including possible side chains or other functional groups. Moreover, we consider an ideally-homogeneous material while in real polyethylene crystalline lamellas are embedded in a globally amorphous material. The oxygen solubility is very different in the two phases [18] and the radio-oxidation kinetics is therefore different in the crystalline and amorphous phases.

2.2. Parameters

The parametrization of such a model is of course a critical issue. In order to limit as much as possible the number of free parameters, we consider mainly diffusion-controlled reactions. We emphasize that this hypothesis is dictated by the sake of consistency. A chemical reaction is necessarily controlled by the encounter of the reactants, which probability is governed by their diffusivity. In any case, the reaction cannot be faster than the encounter realization. In our simulation, the $POO^\bullet$ diffusivity is taken from the work of Pearson *et al.* [19] on long polyethylene chains self-diffusion. For numerical evaluation, we took a chain weight $M_w = 10^5$ $g.mol^{-1}$. Note that we corrected the diffusion coefficient measured at 475 K by an effective Arrhenius law with an activation energy of 23 $kJ.mol^{-1}$ to obtain the diffusion coefficient at 300 K, as suggested in reference [19]. We tentatively assume that the diffusivity of $P^\bullet$ is 10 times larger to account for a possible additional diffusion of radical by hopping. The diffusivity of O_2 in polyethylene is well established [20]. The necessary diffusivity values are summarized in table 1. For a fully diffusion-controlled reaction the link between the reaction constant k and the diffusivity of the two reactants A and B is:

$$k = 4\pi N_A R_{AB} D_{AB} \tag{1}$$

where $D_{AB} = D_A + D_B$ is the sum of the diffusivity of the reactants A and B, R_{AB} is the reaction radius and N_A is the Avogadro number. Note that for two identical reactants, k is often defined by dividing by two the above expression. In the present work we consistently use the definition 1.

The only reaction which is not fully diffusion-controlled is the reaction of the $POO^\bullet$ radical with the polymer PH. In the present case, PH can be considered as a solvent and the above consideration regarding the diffusion does not apply. We thus consider this reaction to be partially diffusion controlled, with a velocity of reaction v. Considering the diffusivity of the PH reactant to be infinite, the link with the reaction rate is given by [10]:

$$k = 4\pi N_A R_{AB}^2 v \frac{D_{AB}}{R_{AB} v + D_{AB}} = 4\pi N_A R_{AB}^2 v \tag{2}$$

The values of the reaction radii R_{AB} and reaction rates are given in table 1. For the partially diffusion-controlled propagatio reaction, we deduced the value of v from the reaction rate reported by Korcek [21] and assuming a C-H bond dissociation energy of 100 $kcal.mol^{-1}$ [22] and a reaction radius $R_{AB} = 0.3$ nm. The reaction constant k is in the lower limit of the values proposed by Korcek [21] and is definitely subject to a large uncertainty. Nevertheless, increasing this parameter over 4 order of magnitudes changes mostly the number of POOH formed in the propagation step while leaving the other products unchanged. In the present case where PH constitutes the bulk of the material, the reaction of $POO^\bullet$ with PH reduces to a first order reaction, with

a characteristic reaction time $\tau^{-1} = kC_{\mathrm{PH}}$, where $C_{\mathrm{PH}} = 68$ mol.dm^{-3} is the concentration of the PH in the material that corresponds to the molar concentration of -CH_2- units in a theoretical polyethylene having a mass density of 0.95 kg.dm^{-3}.

Table 1: parameters for oxidation chemical reactions. D.C.: diffusion-controlled reaction; P.D.C.: partially diffusion-controlled reaction. The reaction radius was deduced from the average volume of a -CH_2- unit in polyethylene. The O_2 diffusion constant was obtained from reference [20]. *For the propagation reaction, the velocity of reaction is $v = 1.5\ 10^{-5}$ nm.s^{-1}

reaction	type	D_A (nm^2.s^{-1})	D_B (nm^2.s^{-1})	R_{AB} (nm)	k (dm^{3}mol^{-1}s^{-1})
$P^\bullet + O_2 \longrightarrow POO^\bullet$	D.C.	$1.0\ 10^3$	$3.1\ 10^7$	0.3	$7.04\ 10^{+7}$
$POO^\bullet + PH \longrightarrow POOH + P^\bullet$	P.D.C.*	$1.0\ 10^2$	$1.0\ 10^2$	0.3	$1.02\ 10^{-5}$
$P^\bullet + P^\bullet \longrightarrow P_2$	D.C.	$1.0\ 10^3$	$1.0\ 10^3$	0.3	$4.54\ 10^{+3}$
$P^\bullet + POO^\bullet \longrightarrow POOP$	D.C.	$1.0\ 10^3$	$1.0\ 10^2$	0.3	$2.49\ 10^{+3}$
$POO^\bullet + POO^\bullet \longrightarrow POOP + O_2$	D.C.	$1.0\ 10^2$	$1.0\ 10^2$	0.3	$4.54\ 10^{+2}$

2.3. Approximate analytical solution for homogeneous condition

In the case of high oxygen concentrations, the oxidation reaction of $P^\bullet$ is much faster than the other reactions. For a homogeneous source term constant in time, the $P^\bullet$ concentration reaches a quasi-stationary value much more quickly than $POO^\bullet$ does. Moreover, the second order termination reactions $P^\bullet + P^\bullet \longrightarrow P_2$ and $P^\bullet + POO^\bullet \longrightarrow POOP$ have a negligible contribution due to their small reaction constant with respect to the oxidation reaction $P^\bullet + O_2 \longrightarrow POO^\bullet$. For the propagation reaction $POO^\bullet + PH \longrightarrow POOH + P^\bullet$, the production of $P^\bullet$ instantaneously produces $POO^\bullet$, so that the net results of the propagation reaction does not modify the $POO^\bullet$ concentration, while producing POOH. The evolution equation for the $POO^\bullet$ radical reduces thus to a second order kinetics:

$$\frac{\partial q}{\partial t} = -k_q q^2 + \sigma \tag{3}$$

where q is the $POO^\bullet$ radical concentration at time t and σ is a source term proportional to the dose rate resulting from the instantaneous reaction of $P^\bullet$ with O_2. The reaction constant k_q controls the second order reaction between two $POO^\bullet$. Note that the definition 1 has been used here, so that no factor 2 appears in the second term of the right-hand side. Setting $q_0^2 = \frac{\sigma}{k_q}$, the integration is straightforward and gives:

$$q(t) = q_0 \tanh\left(k_q q_0 t\right) \tag{4}$$

The above relation will be useful to analyse the simulation kinetics. It shows first that a stationary regime is reached after a time τ such that $\tau^{-1} = \omega = k_q q_0$. The stationary value for q is $q_\infty = q_0$. Within this high O_2 concentration approximation, the stationary value q_∞ is controlled exclusively by the termination reaction $POO^\bullet + POO^\bullet \longrightarrow POOP + O_2$. The concentration of POOP and POOH are obtained by a straightforward analytical integration of equation 4.

It is also interesting to look in more details at the stationary regime [6]. In such a case, the numerical homogeneous problem reduces to a system of two coupled algebraic equations of second degree, which defines

the $P^\bullet$ and $POO^\bullet$ stationary concentrations, p_∞ and q_∞, respectively. For a sufficiently long time after the stationary regime has been established, the ratio of POOH over POOP concentrations is given by:

$$\Lambda = \frac{2\gamma}{k_q q_\infty + 2k_{pq} p_\infty} \tag{5}$$

where k_q is the reaction constant for $POO^\bullet + POO^\bullet \longrightarrow POOP + O_2$, k_{pq} is the reaction constant for $P^\bullet + POO^\bullet \longrightarrow POOP$ and γ is the reaction rate for the first order propagation reaction $POO^\bullet + PH \longrightarrow POOH + P^\bullet$. Notice that Λ is one possible definition of the propagation length. We can distinguish two regimes for POOP formation. The first regime associated to low O_2 concentrations is dominated by the reaction $P^\bullet + POO^\bullet \longrightarrow POOP$, while the second regime associated to high O_2 concentrations is dominated by the reaction $POO^\bullet + POO^\bullet \longrightarrow POOP + O_2$. We can define the limit between these two regimes by considering that the variation of $POO^\bullet$ concentration induced by both reactions equals each other, *i.e.*:

$$k_{pq} p_\infty q_\infty = k_q q_\infty^2 \tag{6}$$

Combining this equation with the mass conservation equation:

$$k_p p_\infty^2 + k_q q_\infty^2 + 2k_{pq} p_\infty q_\infty = \sigma \tag{7}$$

and setting the dimensionless parameter $\eta = \frac{k_q k_p}{k_{pq}}$ we obtain the corresponding POOH over POOP concentrations ratio at the limit between these two regimes:

$$\Lambda_L = \frac{2\sqrt{3+\eta}}{3}\gamma\tau \tag{8}$$

It is important to notice that Λ_L varies with the dose rate proportionally to $\sigma^{-\frac{1}{2}}$ like τ and that it cannot, by definition, depend on the O_2 concentration.

In the limit of high O_2 concentration, $p_\infty \approx 0$ and $q_\infty^2 \approx \frac{\sigma}{k_q}$. Thus, Λ varies like the inverse of the stationary $POO^\bullet$ concentration. Such a dependence comes simply from the difference in the order of the kinetics, *i.e.* first order for POOH formation and second order for POOP formation. Finally, at very low O_2 concentrations, a third kinetic regime prevails dominated by $P^\bullet + P^\bullet \longrightarrow P_2$ and then $q_\infty \approx 0$ and $p_\infty^2 \approx \frac{\sigma}{k_p}$. Note, however, that this latter limit corresponds to the case where both POOH and POOP quantities vanishes and any small perturbation is likely to dominate over the present trend. In a more accurate model taking into account minor processes or existing polymer defects, this limit might thus be significantly modified. In the present model, the ratio Λ scales with the dose rate proportionally to $\sigma^{-\frac{1}{2}}$ for both limits, *i.e.* between high and low O_2 concentration and between low and very low O_2 concentration. However, the dose rate dependence is more complex for intermediate oxygen concentration, as we shall see in section 4.

3. KMC simulation

The Kinetic Monte Carlo (KMC) simulation provides an algorithmic solution to the above problem of diffusion-reaction. It is initiated by sampling a source term, which defines the probability to generate radicals

for a given type of radiation. In the present case, we consider a heterogeneous source made of a random series of single ion impacts. Each impact generates a localized track of radicals along the ion path in a simulation box representing a thin slab of polymer. We impose periodic boundary conditions to the simulation box, which size is chosen sufficiently large to ensure that the radicals cannot diffuse across the box during the simulation time T. Since the simulation time and radical concentration depends on the flux, the box size is adapted to the ion flux. It is typically $2 \times 2 \times 0.1$ μm^3 for a flux $\phi = 10^7$ ions cm^{-2}.s^{-1}. Our simulation mimics ion irradiation for which the overall distribution of impact is homogeneous. The dose rate is controlled by the average frequency of impact $\nu = \phi S$, where S is the surface of the sample. The distribution of time between two impacts is exponential as it should for a series of uncorrelated events and the position distribution on the surface is uniform. For a given macroscopic irradiation time T, the number of impacts on the surface S thus follows a Poisson law.

For a given ion impact on the surface, we consider a simple model of radical distribution. We assume first that the ion propagates in straight line along the $\mathbf{u}_z$ direction perpendicular to the surface. We consider that all the ionizations and excitations generated by the projectile along its path lead eventually to the formation of P$^\bullet$ radicals after a fast stage of electron-hole recombination and C-H bond dissociation. These P$^\bullet$ radicals will react with each other, with the O_2 molecules dissolved in the material and with the radicals generated by previous impacts. The average distance between two generated P$^\bullet$ projected along $\mathbf{u}_z$ is given by the inverse mean free path $\lambda^{-1} = Y \frac{dE}{dz}$, where $\frac{dE}{dz}$ is the ion linear energy transfer (LET) in the polymer and Y is the creation yield per unit of energy. In the present study, the radical yield was set to 0.05 eV^{-1}. As observed for ion irradiation of water, the primary yield of radicals does not depends much on the LET for a broad range of LET [11, 12]. Ion track simulation in water and statistical consideration for semiconductor indicates that the yield of electron-hole pair is of the order of $\frac{1}{cE_{\text{gap}}}$, where E_{gap} is the energy gap between the valence and conduction bands in the material and c is a constant varying between 2 and 3 [23]. In the present study, the yield was arbitrarily set to Y=0.05 eV^{-1}. The LET value and the ion flux defines the dose rate $\dot{D}$ for a given material weight density ρ:

$$\dot{D} = \frac{1}{\rho} \frac{dE}{dz} \phi \tag{9}$$

We shall consider as a heterogeneous case the irradiation by He ions at several fluxes and for several oxygen concentrations. These two parameters are easily controlled experimentally and they could be tuned to make a comparison with simulation. The energy of the He ions was set to 5 MeV to roughly mimic an irradiation by alpha particles emitted by actinides. The typical linear energy transfer (LET) for a 5 MeV He ion penetrating a thin slab of polyethylene (CH_2 units at a mass density of 0.95 g.cm^{-3}) is about 100 keV.μm^{-1}. Its range is typically 34 µm and for a thin slab of 10 μm, as achievable experimentally, the LET variation along the thickness is of the order 15%. For the sake of simplicity, we give the radial distribution of radicals in the plane perpendicular to the ion propagation $\mathbf{u}_z$ a two-dimension Gaussian shape, *i.e.* $p(r) = \frac{r}{2\pi a^2} \exp - \frac{r^2}{2a^2}$. The characteristic radial extension $a = 10$ nm is consistent with simulation of liquid water for ions at the same velocity [24]. It provides a rough estimate for polyethylene with comparable energy gap and mass density. More

elaborate track structure calculation could be used to perform a more realistic simulation as it has been done for water radiolysis simulation [12, 11]. However, our main goal is here to focus on the effect of heterogeneous kinetics rather than predicting radiolysis yields for a specific case, which would depend on the nature of the polymer, on the irradiation parameters and on the chosen kinetic constant.

To simulate homogeneous irradiation at the same dose rate as for heterogeneous irradiation, we simply extent the Gaussian radius to a value much larger than the simulation box size. Combined with the use of periodic boundary conditions, this ensures a homogeneous distribution of generated $P^{\bullet}$ in the simulation box. We also increase simultaneously the flux ϕ and the mean free path λ by a factor 100 to obtain a smooth introduction of the radicals in the sample along the irradiation time T. In such a way, the simulation mimics an ideally homogeneous irradiation, with the same average dose rate $\dot{D}$.

Once some radicals are present in the simulation box, the diffusion-reaction process starts. In our simulation, a macroscopic time step is first sampled to define the time of occurrence of the next impact. This macroscopic time step is divided into a series of microscopic time steps, which allows us to simulate the kinetics in the early stage following an impact, when the reactants are highly concentrated in the track core. For a given microscopic time step t, we calculate the probability of reaction for each reactant present in the simulation box. In the present simulation, we have only second order diffusion-controlled reaction and first order reactions. The probabilities of reaction during a time t are, respectively:

$$W_{AB} = \frac{r}{R_{AB}} \operatorname{erfc}\left(\frac{r - R_{AB}}{2\sqrt{D_{AB}t}}\right) \tag{10}$$

and

$$W_A = \frac{1}{\tau_A} \exp\left(-\frac{t}{\tau_A}\right) \tag{11}$$

where r the distance between the two reactants A and B, and τ_A the characteristic reaction time for the first order reaction of reactant A. These probabilities are sampled by comparison with a random number R uniformly generated between 0 and 1. When the probability is larger than R, the reaction is added to the list of possible reactions during the time step t. The reaction list is then sorted from the most likely to the less likely reaction, *i.e.* from the highest to the lowest probability. If a reactant is involved in several concurrent reactions, only the most likely reaction is retained and the others are discarded. It is necessary to limit as much as possible the number of concurrent reactions and we use a small microscopic time step. It is reset to 5 10^{-7} seconds at each impact but it is allowed to vary in time to improve the numerical efficiency. The growth of the microscopic time step is governed by the number of reactions, which occur during the prescribed time step. If there are less than 5 reactions and if the reaction probability is less than 0.02 the time step is doubled. This growth is limited to time steps lower than 1 second. Note that such a scheme does not eliminate completely the possibility of concurrent reactions for a given radical, though the chosen time step is small with respect to the reaction rate. An alternative algorithm would be to sample the reaction times and to realize only the fastest reactions [10]. The analysis and sampling of the reaction scales as N^2, where N is the number of reactants in the simulation

box. This step forms the main body of the KMC simulation. Using the above described variable time step scheme, we can follow the introduction of a few 10^5 $P^\bullet$ radicals during 10^3 seconds, typically.

Once all reacting pairs in the time step t have been identified, the reactions are realized by placing the reaction products at the barycentre of the diffusion-weighted positions. The vast majority of radicals and molecules do not react during a single time step. For all of these particles, the diffusion process is taken into account by sampling a new position for each of them according to the Fick law of diffusion defined by the particle diffusivity in the polymer.

For high O_2 concentrations, the number of O_2 molecules in the simulation box is too large for the above method to be practical. In this case we use a method originally introduced by Pimblott and used for water radiolysis simulations [25, 26]. It consists in representing the ensemble of O_2 molecules as an homogeneous inexhaustible reservoir of particles. The second order reactions of O_2 with another particle thus reduces to a first order reaction, with a characteristic reaction time τ related to the concentration by the relation $\tau^{-1} = kc_{O_2}$, where k is the reaction constant of the bimolecular reaction. The comparison of this method with the explicit account of all the O_2 molecules dissolved in the box shows that the approximation is accurate down to $c_{O_2} = 10^{-5}$ mM. Below this limit, the O_2 concentration in the track is small and the dissolved O_2 can no longer be considered as an inexhaustible reservoir. Nevertheless, with the present parameterization, the reactions inside the track (uptake and release of O_2) are relatively slow with respect to the oxygen diffusion and an efficient renewal of the oxygen molecules inside the track is thus ensured. For the sake of simplicity we have thus considered the dissolved oxygen as a homogeneous reservoir for all O_2 concentrations simulated in this work.

Since the KMC simulation is a statistical method, the number of products fluctuates from one simulation run to another one. We performed systematically 32 runs to obtain a meaningful average value. Such an averaging procedure is comparable to the experimental approach, which consists in measurements over a sufficiently large volume. In the simulation, each run is representative of a small volume disconnected from the others. An example of the averaging process is depicted in figure 1 which represents the time evolution of the number of $POO^\bullet$ radicals. The red curve corresponds to a single run kinetics. It is made of spikes correlated in time with each ion impact and thus with the spikes observed in the $P^\bullet$ curve represented in blue. Each spike decays according to the reaction kinetics of $POO^\bullet$ in a single ion track. The overall increase of the number of species reflects the accumulation of $POO^\bullet$ with the increase of the number of ion impacts. After some time, the number of $POO^\bullet$ reaches a pseudo-stationary regime characterized by large fluctuations around a slowly varying average curve. The average over 32 such kinetics is depicted by the black curve obtained for an histogram time bin of 1 second. The spikes are no longer visible and this curve represents what could be observed in a macroscopic measurement of the $POO^\bullet$ radicals. The average curve is characterized by a raising time and a plateau value, which depends on the physical parameters of the source term and on the oxygen concentration.

Figures 2 and 3 illustrate the effect of heterogeneity at the nanometre scale. The figure 2 shows a typical realisation of heterogeneous diffusion reaction kinetics for the $POO^\bullet$ radicals when the pseudo-stationary regime has been reached, after 400 seconds. We observe clearly that the distribution is not homogeneous and superimposed to a pseudo homogeneous background, some high-density areas can be observed, in particular in

the upper right corner of the figure and in the left hand side. They correspond obviously to the latest impacts in the simulation box. The color scale indicates the age of the radicals. The distribution of age is dominated by the youngest radicals. For a series of longer He simulation runs, up to 1000 seconds at the same dose rate, the average lifetime of the oldest decile is of the order of 380 seconds and the average lifetime of the youngest decile is as short as 2.5 seconds. The corresponding diffusion lengths are respectively 195 for the oldest decile but only 15 nanometres for the youngest decile. The fluence cumulated during the 380 s period is 3.8 10^9 cm^{-2}, which corresponds to a mean shortest distance between impacts, d_t, of 80 nm. It is interesting to note that the diffusion length of the oldest decile is not much larger than d_t. This indicates that the pseudo homogeneous background observed in fig 2 is not, by far, uniquely due to the radical diffusion but also to the overlapping of tracks. In a liquid, where diffusion coefficients are several orders of magnitude higher, the spatial homogenization origin would be different as mainly ruled by the species diffusion. A similar simulation run performed for a homogeneous irradiation case gives rather similar average lifetimes: 175 s and 2.5 s for the oldest and youngest deciles, respectively. Surprisingly, two spatially very different distributions produce, on the average, quite similar time evolutions.

The distribution $g(R)$ of distance R between two $POO^{\bullet}$ in the plane perpendicular to the ion propagation direction is depicted in figure 3 for several dose rates. Because of the discrete nature of the heterogeneous source term and of the necessarily limited size of the simulation box, the instantaneous radial distribution function does not represent faithfully the stationary distribution. To overcome this limitation, the curves presented in figure 3 were obtained as the average over a time interval corresponding to 20 impacts well after the stationary regime has been established and for 32 simulation runs. Except from statistical fluctuations, all distributions have reached their stationary regime and no longer evolve in time. The curves associated to heterogeneous irradiations deviate significantly from the curve associated to the reference homogeneous case. For the latter, the deviation from a perfect straight line parallel to the abscissa axis comes from statistical fluctuations of the KMC simulation in a box of limited size for one single run. These fluctuations are particularly visible for small R associated to small sampling volumes. For heterogeneous kinetics, it is important to note that the distribution depends on the flux or dose rate, as illustrated in figure 3. We observe clearly that the lower the flux the broader and the higher the distribution. As expected, the heterogeneity is thus stronger for low flux, because in this case the stationary distribution reflects mainly the evolution of individual tracks during a broad distribution of evolution times.

Figures 2 and 3 well show what is stationary regime for an heterogeneous irradiation case. Spatial homogeneity is never reached but there is a temporal stationary regime, in the sense that not only the mean value of the radical concentration is constant in time but also is the average spatial distribution of radicals, *i.e.* the g(R) function. Snapshots, like the one shown on figure 2, taken at different positions or times will always be different but, in average, they depict the same radial distribution. The lower the flux/dose rate is, the higher is the departure from spatial homogeneity.

4. Results

4.1. A typical time evolution

Before investigating the sensitivity to O_2 concentration and dose rate, it is important to look at the time evolution of the various species involved in the radio-oxidation kinetics. For a typical flux $\phi = 10^7$ cm^{-2}.s^{-1}, the corresponding dose rate is $\dot{D} = 6.1$ kGy.h^{-1}. For such a dose rate and for an oxygen concentration $c_{O_2} = 0.2$ mM, we compare in figure 4 the heterogeneous kinetics induced by a series of ion impacts with the homogeneous kinetics at the same dose rate. As noted in section 2.3, the concentration of $P^\bullet$ radicals is on the average negligible for such a high oxygen concentration because the reaction with O_2 is very fast. We can therefore use for the homogeneous case the corresponding analytical expressions for the concentration of $POO^\bullet$, POOP and POOH. As it can be observed on figure 4, the agreement is excellent. The fluctuation of the homogeneous KMC results for $POO^\bullet$ are simply due to the limited box size used in this case.

For $POO^\bullet$ a stationary regime is reached after approximately 100 seconds for the homogeneous case. The heterogeneous kinetics is slower and the stationary regime is reached after 250 seconds. Both curves can be rather well fitted by a second order kinetics law, which gives $N(t) = N_\infty \tanh \omega t$. In the case of a pure second order homogeneous kinetics, as derived in section 2.3 we have $\omega = \sqrt{k\sigma}$ and $N_\infty \propto \sqrt{\frac{\sigma}{k}}$, where k is the reaction constant and $\sigma = \rho Y \dot{D}$ is the source term. A significant difference is observed for the asymptotic value N_∞, which is roughly 2.3 times lower for heterogeneous kinetics than for homogeneous kinetics, for the chosen typical irradiation parameters. It is important to note that the heterogeneous kinetics cannot be simply deduced from the homogeneous model by adjusting the reaction rate k because the reduction of ω and N_∞ cannot be obtained simultaneously. On the contrary, it is possible to define an approximate effective source term σ, which allows us to reproduce the heterogeneous kinetics with the help of the above formula deduced from homogeneous kinetics. The observed difference between the two kinetics reveals the increase of $POO^\bullet$ consumption, which results from spatially correlated generation of radicals along the ion track.

The yields of POOP are quite comparable for both kinetics. There is however a small but significant difference originating from the early time evolution. The amount of POOP grows linearly with the time for heterogeneous kinetics because of in-track $POO^\bullet + POO^\bullet$ reactions. For homogeneous kinetics, this reactions do not occur until a significant amount of $POO^\bullet$ has been created in the sample. As a result, the amount of POOP grows quadratically at early time and then linearly when the stationary regime is established for $POO^\bullet$, *i.e.*. after 100 seconds with the chosen parameters. The long time growth of POOP is rather similar for both kinetics. This remarkable behavior is due to the mass conservation, which holds irrespectively of the homogeneous or heterogeneous nature of the irradiation. It is important to note that the amount of POOP is larger in the heterogeneous case than in the homogeneous case, despite the larger concentration of $POO^\bullet$ in the homogeneous kinetics case. This is, once more, the effect of spatial correlation for ion irradiation, which results in a higher rate of $POO^\bullet + POO^\bullet$ reactions.

The formation of POOH reveals more the differences inherited from the $POO^\bullet$ kinetics. Actually the POOH formation by means of the first order kinetics is slow and the amount of POOH becomes significant after the stationary regime has been reached for $POO^\bullet$. Because of the first order reaction for propagation, the growth

of POOH reflects directly the amount of available $POO^\bullet$, in contrast to POOP, and the homogeneous and heterogeneous kinetics are different by approximately the same factor 2.3, except for a barely visible difference at early times.

4.2. Sensitivity to O_2 concentration

We present in this section the sensitivity of the results to O_2 concentration for a dose rate of 6 kGy h^{-1}, *i.e.* a flux $\phi = 10^7$ ions cm^{-2} s^{-1} for 5 MeV He ions. We analyse here the yields defined as the number of species per 100 deposited eV when the stationary regime is established. For $POO^\bullet$, this definition of the yield is meaningless and we have instead reported the stationary concentration. In the present case, each simulation run lasts 10^3 seconds and the stationary yields of the termination products are obtained by averaging from $2\ 10^2$ to 10^3 seconds over 32 runs.

For the heterogeneous yields depicted in the upper panel of figure 5, we observe clearly the saturation of both $POO^\bullet$ and POOH formation for $c_{O_2} > 2\ 10^{-5}$ mM. The total yield of POOH is however much smaller than the yield of the other termination products. Regarding POOP, we observe a saturation for $c_{O_2} > 2\ 10^{-2}$ mM approximately, while P_2 is no longer formed. This threshold is controlled by the very fast consumption of $P^\bullet$ in this range of O_2 concentration. The relative formation of P_2 and POOP exhibits a clear anti-correlation, as expected in the present model. Whatever the nature of the kinetics, homogeneous or heterogeneous, this anti-correlation results from mass conservation, which can be expressed as $2Y_{P_2} + 2Y_{POOP} = Y_R$, where Y_R is the radical creation yield. This can be observed in the upper panel of figure 5, where the sum of the termination product yields does not change significantly with O_2 concentration, except for small unavoidable statistical fluctuations due to the KMC method. The termination product yield is thus equal to 2.5 for 100 deposited eV, *i.e.* half of the $P^\bullet$ radical creation yield in the present simulation.

The variation of the ratio $\Lambda = Y_{POOH}/Y_{POOP}$ is depicted in the lower panel of figure 5. The black triangles show the simulation results for homogeneous kinetics, which agrees fairly well with the numerical evaluation of the stationary yield obtained by solving the two coupled non-linear equations defining the stationary regime. In the homogeneous case, the variation of Λ is controlled by the relative values of the reaction rates of $P^\bullet + POO^\bullet \longrightarrow POOP$ and $POO^\bullet + POO^\bullet \longrightarrow POOP + O_2$ as discussed in section 2.3. We can distinguish three regimes defined by the two plateaus and the transition between them. At low O_2 concentration the lifetime of $P^\bullet$ is long enough for the first reaction to occur. The $POO^\bullet$ concentration remains low however, and the dominant radical reaction is $P^\bullet + P^\bullet \longrightarrow P_2$. This regime corresponds to the lowest-level plateau observed in figure 5. At high O_2 concentration on the contrary, the concentration of $P^\bullet$ vanishes and only the second reaction takes place, defining the highest-level plateau in figure 5. In the intermediate regime, the first reaction is progressively replaced by the second as c_{O_2} increases.

In the heterogeneous case, the diffusion and the spatial distribution of reactants play a significant role and in the present case they change significantly the variation of the ratio Λ with the O_2 concentration. The ratio depicted by red dots in figure 5 exhibits a well-defined maximum around $c_{O_2} = 2\ 10^{-6}$ mM. With the chosen model parameters, at the same dose rate for homogeneous kinetics, the $POO^\bullet$ yield is roughly 2.3 larger

and we might expect the propagation chain length to be proportionally shorter because the ratio Λ varies proportionally to the inverse of the $POO^\bullet$ concentration in the homogeneous stationary regime as discussed in section 2.3. For very low O_2 concentration we observe indeed that the ratio Λ is larger by a factor 3 approximately. This result can be understood as follows. In ion track, the early reaction stage is dominated by the reaction $P^\bullet + P^\bullet \longrightarrow P_2$, and only very few $POO^\bullet$ radicals are eventually generated. The accumulation of tracks is thus similar to homogeneous generation of $POO^\bullet$ at a lower equivalent dose rate. The stationary concentration reached in such conditions is thus lower, which produces a higher ratio. Moreover, Λ increases with c_{O_2} just like for the homogeneous irradiation in this low O_2 concentration regime. This is no longer the case when the O_2 concentration becomes large as observed in figure 5 for $c_{O_2} > 2\ 10^{-6}$ mM. The higher oxidation rate favours the formation of $POO^\bullet$, which reacts in the track with the other radicals to form POOP. As the in-track concentration of available $POO^\bullet$ increases with O_2 concentration the second order elimination reaction $POO^\bullet + POO^\bullet \longrightarrow POOP + O_2$ takes over the first order propagation reaction $POO^\bullet + PH \longrightarrow POOH + P^\bullet$. This is clearly seen in the upper panel of figure 5 where the saturation of Y_{POOH} is reached long before the saturation of Y_{POOP}. As a result, Λ decreases with c_{O_2} until both yields have reached their saturation value.

Finally, the length of the propagation chain is rather short in the present case of relatively high dose rate. For homogeneous kinetics under saturated O_2 concentration we have $\Lambda \approx 7.2\ 10^{-2}$ as expected from section 2.3, while or heterogeneous kinetics we obtain $\Lambda \approx 2.9\ 10^{-2}$. The actual value of the ratio Λ depends of course of the model parameters. In particular, increasing the propagation reaction rate increases Λ. However, the observed behaviour remains the same as long as the propagation reaction constant remains significantly smaller than the termination reaction constant. By increasing the propagation rate by 4 orders of magnitude, the values of Λ becomes 720 and 235 for homogeneous and heterogeneous case, respectively, under saturated O_2 condition.

This is another illustration of the heterogeneous kinetics, for which the higher $POO^\bullet$ concentration in tracks activates the formation of POOP, while the average $POO^\bullet$ concentration is lower. Another choice of the reaction constants could of course produce a different variation of this ratio with respect to c_{O_2}. However, the difference between homogeneous and heterogeneous irradiation should remain observable, as it is a property of the source term rather than a property of the model itself. Likewise, changing the $P^\bullet$ distribution profile, by varying the ion LET for example, could magnify or reduce the difference between homogeneous and heterogeneous kinetics regarding the ratio Λ.

4.3. Sensitivity to dose rate

We have investigated the sensitivity to the dose rate for a fixed O_2 concentration $c_{O_2} = 2\ 10^{-1}$ mM corresponding to atmospheric pressure of air for the solubility given in reference [18]. The simulation results are reported in figure 6 for three different dose rates: $6.1\ 10^{-4}$, 6.1 and $6.1\ 10^2$ kGyh^{-1} corresponding to ion fluxes 10^3, 10^7 and 10^9 cm^{-2}s^{-1}, respectively. To make the comparison easier, we have made use of the scaling law suggested in section 2.3. The time is thus multiplied by $\sqrt{\frac{\phi}{\phi_0}}$ and for the $POO^\bullet$ radicals the number of particles is scaled by $\sqrt{\frac{\phi}{\phi_0}}$. We use $\phi_0 = 10^7$ cm^{-2}s^{-1} as a reference flux. As expected for homogeneous kinetics, the curves obtained for different dose rates merge in one single curve, except for weak statistical fluctuation of the

KMC method. The three simulated curves agree well with the simplified analytic estimate given in section 2.3 for both $POO^\bullet$ and POOH. Only the curves at the reference flux are shown here for the sake of clarity.

For heterogeneous kinetics the scaled curves associated to the three dose rates have quite similar shapes. Nevertheless, we observe a clearly visible deviation from perfect scaling. The dose rate increase leads to an increase of $POO^\bullet$ concentration, which in turn leads to an increase of the POOH formation. Such a small increase of the POOH yield with the dose rate might be observed experimentally, provided a sufficiently broad range of dose rates can be accessed. This effect is a manifestation of the heterogeneous kinetics. In this case, the dose rate increase reduces the average time between two impacts. The diffusion of $POO^\bullet$ radicals is therefore limited between two impacts and a higher average scaled number of particle per track is reached. This effect is sensitive to the diffusivity of the reactant and should reduce when the reactant diffusivity increases.

To analyze the propagation kinetics, we have plotted in figure 7 the variation of the ratio Λ with respect to O_2 concentration for 3 selected dose rates: 6.1 10^{-4}, 6.1 and 6.1 10^2 $kGyh^{-1}$ corresponding to ion fluxes 10^3, 10^7 and 10^9 $cm^{-2}s^{-1}$, respectively. According to the analysis presented in section 2.3, Λ is scaled by the ratio $\sqrt{\frac{\phi}{\phi_0}}$. Considering homogeneous irradiation first, we observed the expected scaling at the two ends of the c_{O_2} range, where the scaled ratio Λ reaches the same limits whatever the dose rate. The KMC results follow very well the curves deduced from the analysis presented in section 2.3. For the sake of clarity only one KMC simulation result is plotted at the intermediate dose rate. As discussed in the previous section, the low c_{O_2} limit corresponds to termination by the reaction $P^\bullet + POO^\bullet \longrightarrow POOP$ while the high c_{O_2} limit corresponds to the termination reaction $POO^\bullet + POO^\bullet \longrightarrow POOP + O_2$. The separation between these two regimes is defined by $\Lambda_{L0} = 4.4\ 10^{-2}$, which is independent on the flux due to the rescaling by $\sqrt{\frac{\phi}{\phi_0}}$. The crossing between this straight line and the curve $\Lambda(c_{O_2})$ defines, for each corresponding flux, the limit between high and low O_2 concentrations for homogeneous kinetics. The dose rate increase leads mainly to a curve translation, which corresponds approximately to a rescaling of the O_2 concentration by a factor depending on the flux. We observe thus that the termination reaction regime changes with the flux for a given O_2 concentration.

Considering now the results obtained for heterogeneous irradiation, we observed a significant difference with the homogeneous case. For a given flux, the variation of Λ with c_{O_2} exhibits a well defined maximum as discussed in the previous section. This maximum position is approximately located at the c_{O_2} value where, for the homogeneous case, the curves $\Lambda(c_{O_2})$ cross Λ_{L0}, which indicates the transition between the two POOP formation regimes with O_2 concentration. For large c_{O_2}, Λ is smaller in the heterogeneous case than in the homogeneous case, whatever the dose rate. This reveals the large number of $POO^\bullet$+$POO^\bullet$ reactions in the track core. For low c_{O_2} on the contrary, the propagation is more efficient for the heterogeneous case, in particular at low dose rate. In such a case, the kinetics is dominated by single track evolution and the few $POO^\bullet$ that escape the track are very active to react with the virgin polymer and to form POOH before radicals created by another track may react with them and stop the propagation process. This effect reduces progressively as the dose rate increases, because the duration of the propagation process is limited by the average time between two impacts. For heterogeneous kinetics, high dose rate is thus to some extent more similar to the homogeneous case, as it was observed also for the radial distribution discussed at the end in section 3.

Whether these trends can be observed experimentally is of course an important question for our understanding of polymer ageing under irradiation. A series of experiments at several flux and for a broad range of O_2 concentration would be very useful to explore the trends observed in the present KMC simulation. Existing literature is far from complete in this respect.

5. Conclusion

In this work we set up a kinetic Monte Carlo (KMC) simulation of polymer radio-oxidation for a synthetic but still realistic model involving two reactive radicals, $P^\bullet$ and $POO^\bullet$, and the main termination products P_2, POOP and POOH. The simulation allows us to investigate a prototype of heterogeneous kinetics induced by penetration of swift light ions in a polymer and to compare it with the reference homogeneous case.

There is a profound effect regarding the nature of the stationary regime established after a sufficient long time of irradiation. In the case of heterogeneous kinetics, we do not observe the progressive homogenization of the $POO^\bullet$ radical concentration. The distribution function of the $POO^\bullet$ inter-particle distance remains peaked at short distances and the average concentration is significantly lower. However the time evolution of the average $POO^\bullet$ radical concentration at the macroscopic scale exhibits a similar shape in both homogeneous and heterogeneous cases. In the high O_2 concentration regime, the relative variation of the $POO^\bullet$ stationary concentration with the dose rate $\dot{D}$ deviates slightly from the perfect scaling given by $\sqrt{\dot{D}}$ in the homogeneous case.

The difference between heterogeneous and homogeneous kinetics can be traced back by looking at the yield variation with respect to oxygen concentration. In particular the yield ratios $\Lambda = \frac{Y_{\mathrm{POOH}}}{Y_{\mathrm{POOP}}}$ are significantly different from each other. The propagation associated to POOH formation under saturated oxygen condition is severely reduced in the case of heterogeneous kinetics investigated here, in particular in the low dose rate regime. Note that using a larger propagation rate does not change this conclusion as it would mainly scale Λ proportionally to propagation rate increase.

The oxygen concentration and the dose rate are the most easily tunable physical parameters to analyse polymer radio-oxidation. The simulation predicts significant yield variations with respect to both parameters and it is certainly worth to investigate such variation experimentally to analyse the degree of heterogeneity in the radio-oxidation kinetics. Our simulations show that the built-up regime of the stationary state span over tens of seconds. It is thus sufficiently slow to be observed experimentally by standard means. In particular a direct measurement of the $P^\bullet$ and $POO^\bullet$ by means of ESR spectroscopy would be extremely beneficial to benchmark the KMC simulation and to improve our understanding of the radio-oxidation process. Besides, measuring the time evolution of the POOP during the first tens of seconds is also an interesting option for revealing the role of heterogeneity.

Looking now to possible comparison with experimental data, it is probably difficult to achieve an ideally homogeneous irradiation as considered here [27]. If we consider as a reference case high-energy photon irradiation, the photoelectric and Compton effects governing their absorption in matter generates primary electrons with an energy of the order of a few tens of keV. The resulting ionization track is made of a series of spatially

correlated events rather than uniformly distributed impacts. Such kind of irradiation should be considered as a combination of both homogeneous and heterogeneous kinetics. A detailed investigation of the track structure is thus desirable to enable a direct comparison with experiments. In the same spirit, ion irradiation also ejects fast electrons, sometimes called delta rays, which escape the center of the track, creating thus less dense concentration of radicals with respect to the ideal Gaussian distribution used in the present case. Nevertheless, ion irradiation allows us to tune the radical density in the track by changing the projectile characteristics. This allows us to vary the dose rate by changing either the flux or the energy release per impact. It should thus be possible to perform a relative comparison between experiment and simulation to investigate the significance of the radical density created in a track.

References

[1] D. C. Phillips and S. G. Burnay, "Polymers in the nuclear power industry," in *Irradiations Effects on Polymers* (D. W. Clegg and A. Collyer, eds.), ch. 9, pp. 345–381, Elsevier Applied Science, 1991.

[2] J. L. Bolland and G. Gee, "Kinetic studies in the chemistry of rubber and related materials. ii. the kinetics of oxidation of unconjugated olefins," *Trans. Faraday Soc.*, vol. 42, pp. 236–243, 1946.

[3] M. Ferry, G. Roma, F. Cochin, S. Esnouf, V. Dauvois, F. Nizeyimana, B. Gervais, and Y. Ngono-Ravache, "3.16 - polymers in the nuclear power industry," in *Comprehensive Nuclear Materials (Second Edition)* (R. J. Konings and R. E. Stoller, eds.), pp. 545 – 580, Oxford: Elsevier, second edition ed., 2020.

[4] L. Audouin, V. Gueguen, A. Tcharkhtchi, and J. Verdu, ""close loop" mechanistic schemes for hydrocarbon polymer oxidation," *Journal of Polymer Science Part A: Polymer Chemistry*, vol. 33, no. 6, pp. 921–927, 1995.

[5] A. François-Heude, E. Richaud, A. Guinault, E. Desnoux, and X. Colin, "Impact of oxygen transport properties on polypropylene thermal oxidation, part 1: Effect of oxygen solubility," *Journal of Applied Polymer Science*, vol. 132, no. 5, 2015.

[6] K. T. Gillen, J. Wise, and R. L. Clough, "General solution for the basic autoxidation scheme," *Polymer Degradation and Stability*, vol. 47, no. 1, pp. 149 – 161, 1995.

[7] K. T. Gillen, J. Wise, and R. L. Clough, "Accelerated aging methods for predicting long-term mechanical performance of polymers," in *Irradiations Effects on Polymers* (D. W. Clegg and A. Collyer, eds.), ch. 4, pp. 157–223, Elsevier Applied Science, 1991.

[8] G. R. Freeman, "Nonhomogeneous kinetics in irradiated liquids," *International Journal for Radiation Physics and Chemistry*, vol. 4, no. 2, pp. 237 – 248, 1972.

[9] K. T. Gillen and R. L. Clough, "Quantitative confirmation of simple theoretical models for diffusion-limited oxidation," in *Radiation Effects on Polymers*, ch. 28, pp. 457–472, 1991.

[10] N. J. B. Green, M. J. Pilling, S. M. Pimblott, and P. Clifford, "Stochastic modeling of fast kinetics in a radiation track," *The Journal of Physical Chemistry*, vol. 94, no. 1, pp. 251–258, 1990.

[11] V. Cobut, Y. Frongillo, J. P. Patau, T. Goulet, M.-J. Fraser, and J.-P. Jay-Gérin, "Monte carlo simulation of fast electron andproton tracks in liquid water*i[physical and physicochemical aspects," *Radiation Physics and Chemistry*, vol. 51, no. 3, pp. 229 – 243, 1998.

[12] B. Gervais, M. Beuve, G. Olivera, and M. Galassi, "Numerical simulation of multiple ionization and high let effects in liquid water radiolysis," *Radiation Physics and Chemistry*, vol. 75, no. 4, pp. 493 – 513, 2006.

[13] G. P. Horne, T. A. Donoclift, H. E. Sims, R. M. Orr, and S. M. Pimblott, "Multi-scale modeling of the gamma radiolysis of nitrate solutions," *The Journal of Physical Chemistry B*, vol. 120, no. 45, pp. 11781–11789, 2016. PMID: 27779879.

[14] V. L. Klochikhina and L. I. Trakhtenberg, "Fluctuation effects in the solid-phase kinetics of diffusion-controlled radiation-chemical processes: A monte carlo simulation," *High Energy Chemistry*, vol. 44, pp. 261–267, 2010.

[15] A. V. Tobolsky, "Oxidative degradation of polymeric material," *Discuss. Faraday Soc.*, vol. 2, pp. 384–388, 1947.

[16] R. L. Clough and K. T. Gillen, "Radiation-oxidation of polymers," *Proceedings of a final research co-ordination meeting organized by the international atomic energy agency*, pp. 11–24, 1989.

[17] G. Gryn'ova, J. L. Hodgson, and M. L. Coote, "Revising the mechanism of polymer autooxidation," *Org. Biomol. Chem.*, vol. 9, pp. 480–490, 2011.

[18] A. S. Michaels and H. J. Bixler, "Solubility of gases in polyethylene," *Journal of Polymer Science*, vol. 50, no. 154, pp. 393–412, 1961.

[19] D. S. Pearson, G. Ver Strate, E. Von Meerwall, and F. C. Schilling, "Viscosity and self-diffusion coefficient of linear polyethylene," *Macromolecules*, vol. 20, no. 5, pp. 1133–1141, 1987.

[20] A. S. Michaels and H. J. Bixler, "Flow of gases through polyethylene," *Journal of Polymer Science*, vol. 50, no. 154, pp. 413–439, 1961.

[21] S. Korcek, J. H. B. Chenier, J. A. Howard, and K. U. Ingold, "Absolute rate constants for hydrocarbon autoxidation. xxi. activation energies for propagation and the correlation of propagation rate constants with carbon–hydrogen bond strengths," *Canadian Journal of Chemistry*, vol. 50, no. 14, pp. 2285–2297, 1972.

[22] S. J. Blanksby and G. B. Ellison, "Bond dissociation energies of organic molecules," *Accounts of Chemical Research*, vol. 36, no. 4, pp. 255–263, 2003. PMID: 12693923.

[23] C. A. Klein, "Bandgap dependence and related features of radiation ionization energies in semiconductors," *Journal of Applied Physics*, vol. 39, no. 4, pp. 2029–2038, 1968.

[24] M. Waligórski, R. Hamm, and R. Katz, "The radial distribution of dose around the path of a heavy ion in liquid water," *International Journal of Radiation Applications and Instrumentation. Part D. Nuclear Tracks and Radiation Measurements*, vol. 11, no. 6, pp. 309 – 319, 1986.

[25] S. M. Pimblott, M. J. Pilling, and N. J. Green, "Stochastic models of spur kinetics in water," *International Journal of Radiation Applications and Instrumentation. Part C. Radiation Physics and Chemistry*, vol. 37, no. 3, pp. 377 – 388, 1991.

[26] A. Colliaux, B. Gervais, C. Rodriguez-Lafrasse, and M. Beuve, "O2 and glutathione effects on water radiolysis:a simulation study," *Journal of Physics: Conference Series*, vol. 261, p. 012007, jan 2011.

[27] Y. Tabata, "Heterogeneous nature of radiation effect on polymers," in *Irradiation of Polymeric Materials*, ch. 3, pp. 27–49, 1993.

6. Figure captions

Figure 1: Heterogeneous kinetics of polymer radio-oxidation for He irradiation at a flux $\phi = 10^7$ ions $cm^{-2}s^{-1}$ and an O_2 concentration $c_{O_2} = 2\ 10^{-1}$ mM. The curves labeled P and POO x1 were obtained for 1 single KMC run. The curve labeled POO x32 is an average over 32 runs.

Figure 2: Two dimensional distribution of $POO^\bullet$ radicals for a single simulation run of He irradiation during 400 s at a flux $\phi = 10^7$ $cm^{-2}s^{-1}$ and an O_2 concentration $c_{O_2} = 2\ 10^{-1}$ mM. The projection plane is perpendicular to the ion propagation direction. The slab thickness is 0.1 μm. The cumulated fluence is $\phi = 4\ 10^9$ cm^{-2}, corresponding to 40 impacts in the frame. The color scale indicates the age of the radical in seconds.

Figure 3: Radial distribution functions of $POO^\bullet$ radicals in the plane perpendicular to the ion propagation direction. The homogeneous reference case corresponds to one single run for a dose rate equivalent to a flux $\phi = 10^7$ $cm^{-2}s^{-1}$. All heterogeneous curves were normalized to the average stationary concentration and scaled by a factor $\sqrt{\phi}$. In all cases the oxygen concentration is $c_{O_2} = 2\ 10^{-1}$ mM. The $g(R)$ function corresponds to the radii distribution divided by R.

Figure 4: $POO^\bullet$, POOH and POOP kinetics at a flux $\phi = 10^7$ $cm^{-2}s^{-1}$and an oxygen concentration $c_{O_2} = 2\ 10^{-1}$ mM. The homogeneous case depicted in black corresponds to the same dose rate. The analytical result of the simplified kinetics model assuming large c_{O_2} is reported as thick lines for the three chemical species. The simulation box size is 0.4 μm^3.

Figure 5: Upper panel: termination product and consummation yields as a function of oxygen concentration for heterogeneous kinetics with flux $\phi = 10^7$ $cm^{-2}s^{-1}$. (dose rate 6.1 $kGy.h^{-1}$). Note that the yield is meaningless for $POO^\bullet$ and we have plotted instead a number proportional to the stationary concentration with a linear scale. The curve depicted $-O_2$ corresponds to the oxygen uptake yield defined as $Y_{-O_2} = Y_{POOP} + Y_{POOH}$. Lower panel: yield ratio $\Lambda = Y_{POOH}/Y_{POOP}$for homogeneous and heterogeneous kinetics at the same dose rate.

Figure 6: Dose rate sensitivity for homogeneous and heterogeneous kinetics at three different dose rates: 6.1 10^{-4} (a), 6.1 (b) and 6.1 10^2 (c) $kGy.h^{-1}$ corresponding respectively to flux ϕ equal to 10^3, 10^7 and 10^9 $cm^{-2}s^{-1}$. Upper panel: scaled $POO^\bullet$ concentration versus scaled time. Lower panel: POOH concentration versus scaled time. The reference flux is $\phi_0 = 10^7$ $cm^{-2}s^{-1}$. Oxygen concentration $c_{O_2} = 2\ 10^{-1}$ mM. The

homogeneous case are the black curves; for $POO^{\bullet}$, analytical and KMC results are plotted.

Figure 7: Normalized yield ratio $\Lambda\sqrt{\frac{\phi}{\phi_0}}$ for homogeneous and heterogeneous kinetics at three different dose rates: 6.1 10^{-4} (a), 6.1 (b) and 6.1 10^{2} (c) kGy.h^{-1} corresponding respectively to flux ϕ equal to 10^3, 10^7 and 10^9 cm^{-2}s^{-1}. The reference flux is $\phi_0 = 10^7$ cm^{-2}s^{-1}.

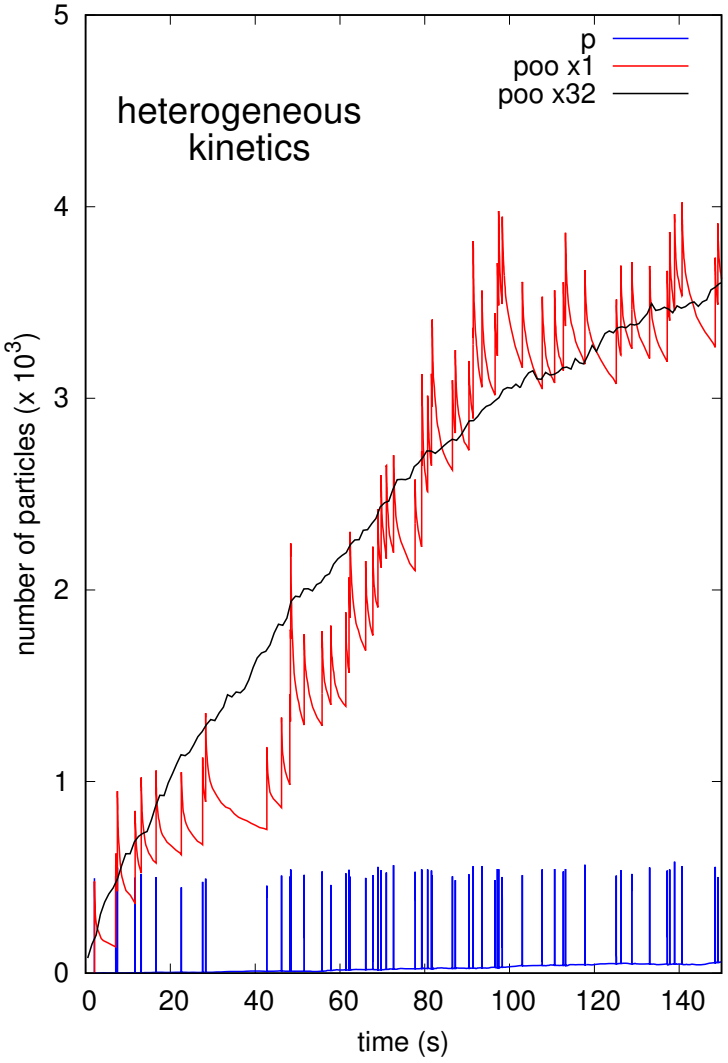

Figure 1: Heterogeneous kinetics of polymer radio-oxidation for He irradiation at a flux $\phi = 10^7$ ions $cm^{-2}s^{-1}$ and an O_2 concentration $c_{O_2} = 2\ 10^{-1}$ mM. The curves labeled P and POO x1 were obtained for 1 single KMC run. The curve labeled POO x32 is an average over 32 runs.

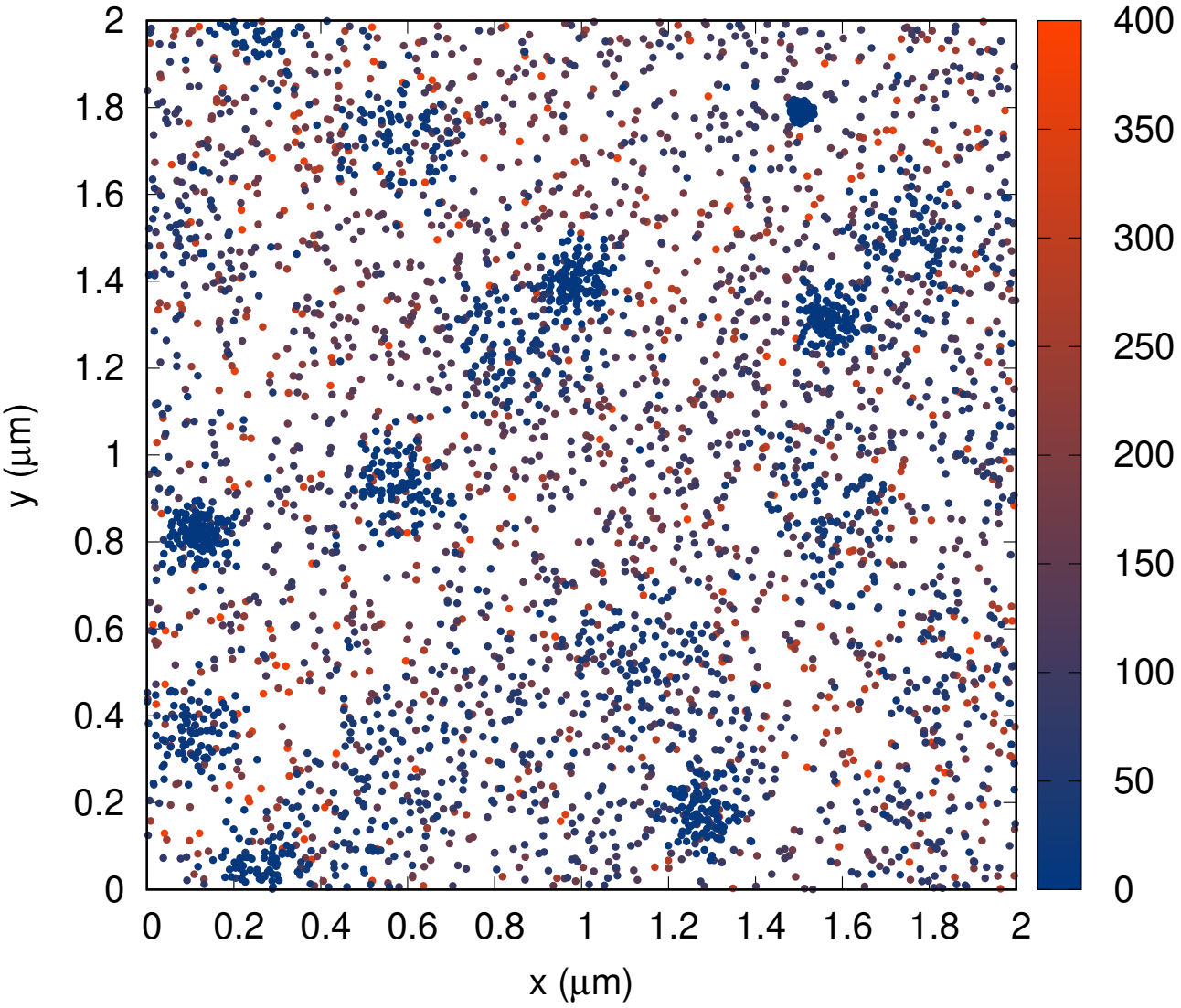

Figure 2: Two dimensional distribution of $POO^{\bullet}$ radicals for a single simulation run of He irradiation during 400 s at a flux $\phi = 10^7$ cm^{-2}s^{-1} and an O_2 concentration $c_{O_2} = 2\ 10^{-1}$ mM. The projection plane is perpendicular to the ion propagation direction. The slab thickness is 0.1 μm. The cumulated fluence is $\phi = 4\ 10^9$ cm^{-2}, corresponding to 40 impacts in the frame. The color scale indicates the age of the radical in seconds.

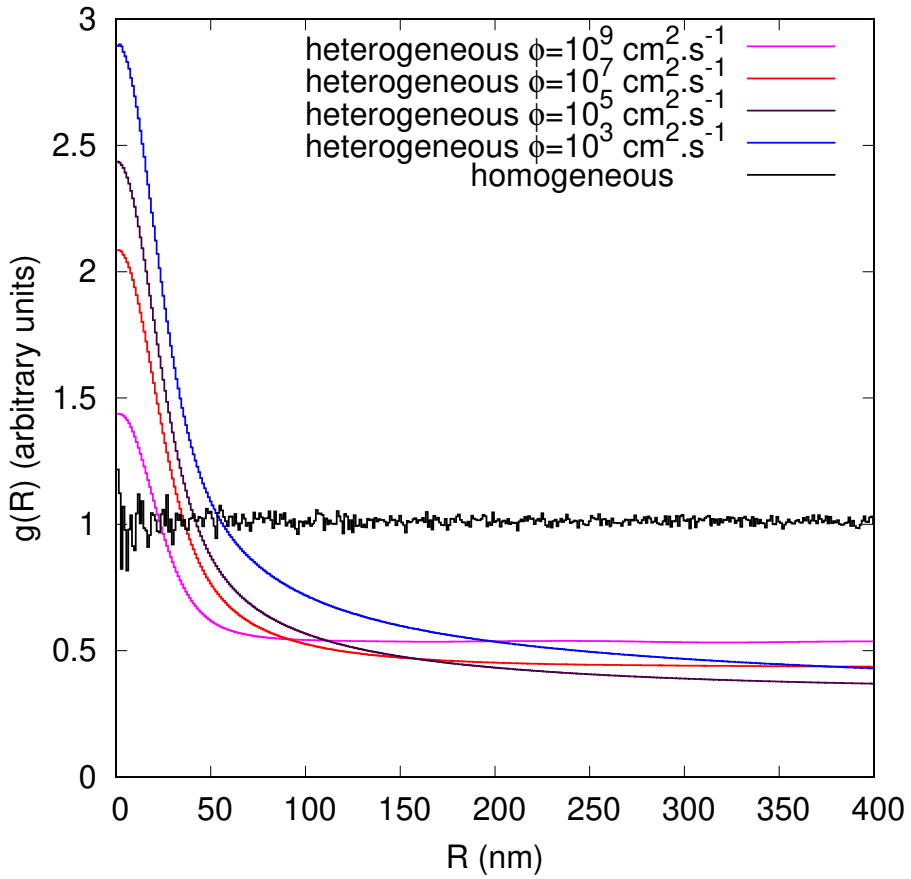

Figure 3: Radial distribution functions of $POO^{\bullet}$ radicals in the plane perpendicular to the ion propagation direction. The homogeneous reference case corresponds to one single run for a dose rate equivalent to a flux $\phi = 10^7$ cm^{-2}s^{-1}. All heterogeneous curves were normalized to the average stationary concentration and scaled by a factor $\sqrt{\phi}$. In all cases the oxygen concentration is $c_{O_2} = 2\ 10^{-1}$ mM. The $g(R)$ function corresponds to the radii distribution divided by R.

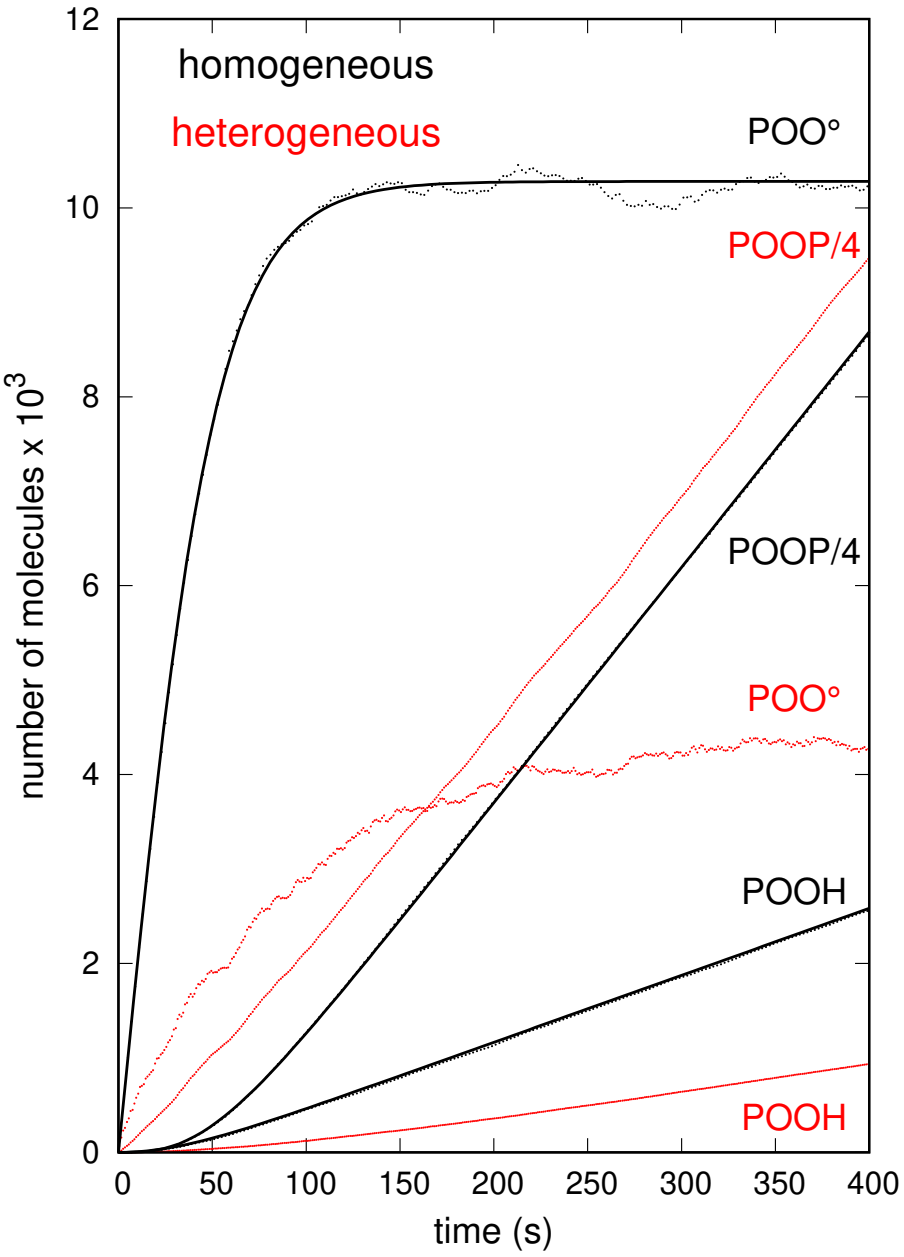

Figure 4: POO$^\bullet$, POOH and POOP kinetics at a flux $\phi = 10^7$ cm^{-2}s^{-1}and an oxygen concentration $c_{O_2} = 2\ 10^{-1}$ mM. The homogeneous case depicted in black corresponds to the same dose rate. The analytical result of the simplified kinetics model assuming large c_{O_2} is reported as thick lines for the three chemical species. The simulation box size is 0.4 μm^3.

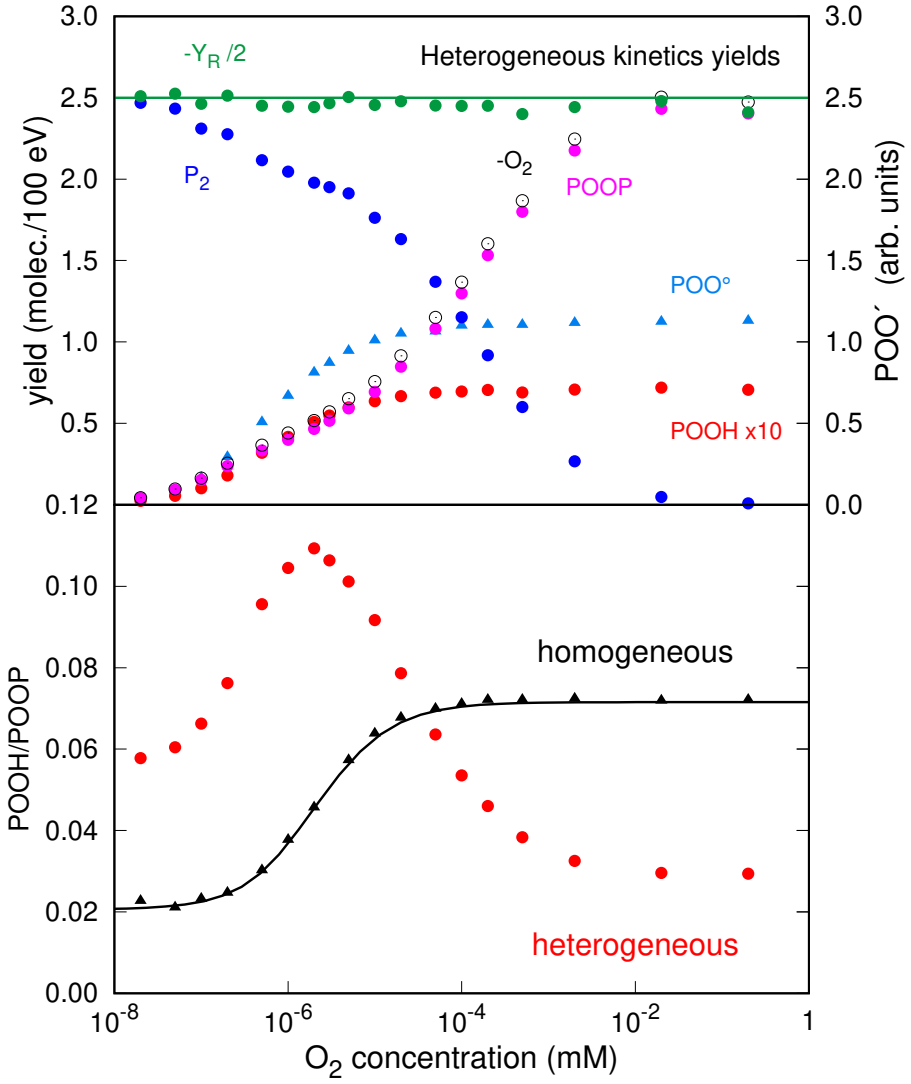

Figure 5: Upper panel: termination product and consummation yields as a function of oxygen concentration for heterogeneous kinetics with flux $\phi = 10^7$ cm^{-2}s^{-1}. (dose rate 6.1 kGy.h^{-1}). Note that the yield is meaningless for POO$^\bullet$ and we have plotted instead a number proportional to the stationary concentration with a linear scale. The curve depicted $-O_2$ corresponds to the oxygen uptake yield defined as $Y_{-O_2} = Y_{POOP} + Y_{POOH}$. Lower panel: yield ratio $\Lambda = Y_{POOH}/Y_{POOP}$for homogeneous and heterogeneous kinetics at the same dose rate.

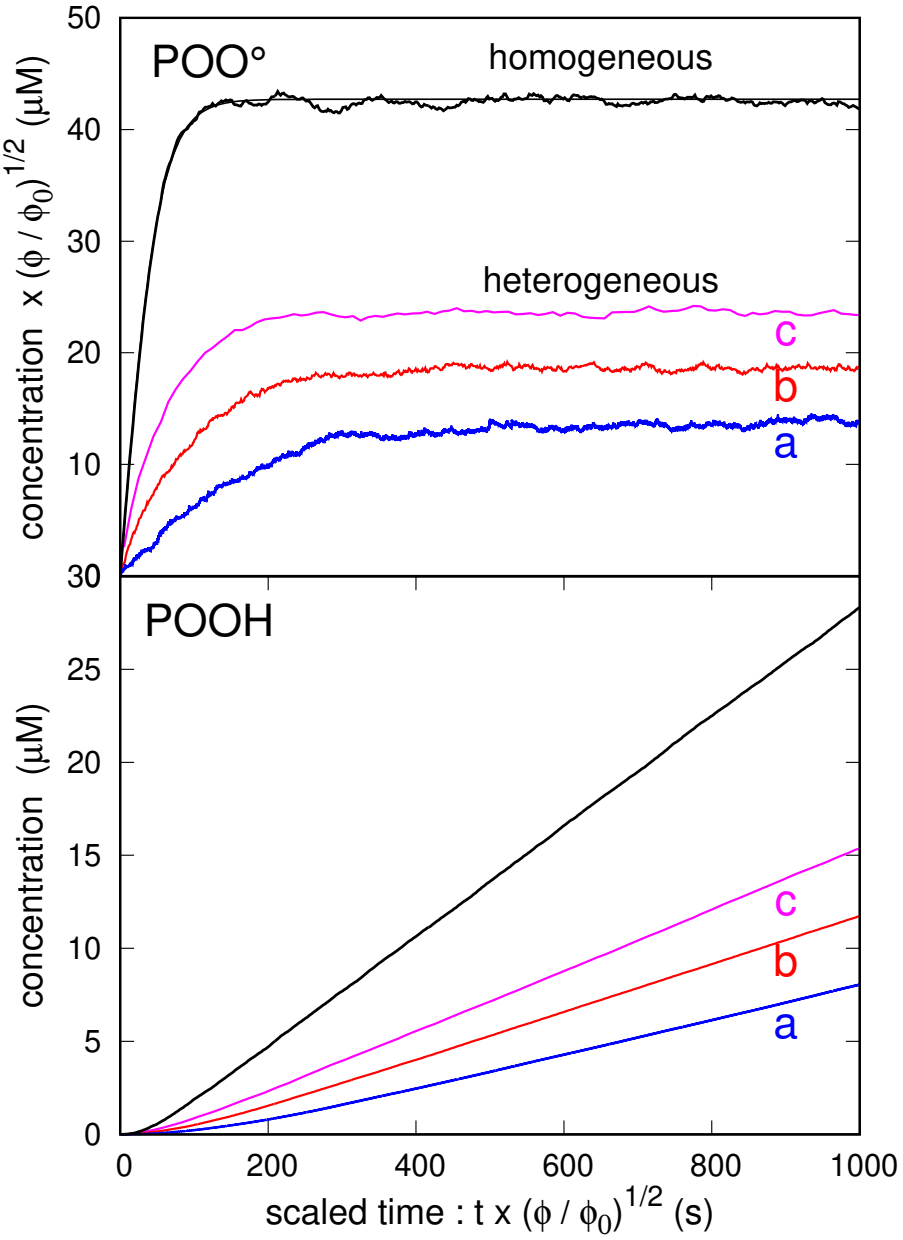

Figure 6: Dose rate sensitivity for homogeneous and heterogeneous kinetics at three different dose rates: 6.1 10^{-4} (a), 6.1 (b) and 6.1 10^{2} (c) kGy.h^{-1} corresponding respectively to flux ϕ equal to 10^3, 10^7 and 10^9 cm^{-2}s^{-1}. Upper panel: scaled POO$^{\bullet}$ concentration versus scaled time. Lower panel: POOH concentration versus scaled time. The reference flux is $\phi_0 = 10^7$ cm^{-2}s^{-1}. Oxygen concentration $c_{O_2} = 2\ 10^{-1}$ mM. The homogeneous case are the black curves; for POO$^{\bullet}$, analytical and KMC results are plotted.

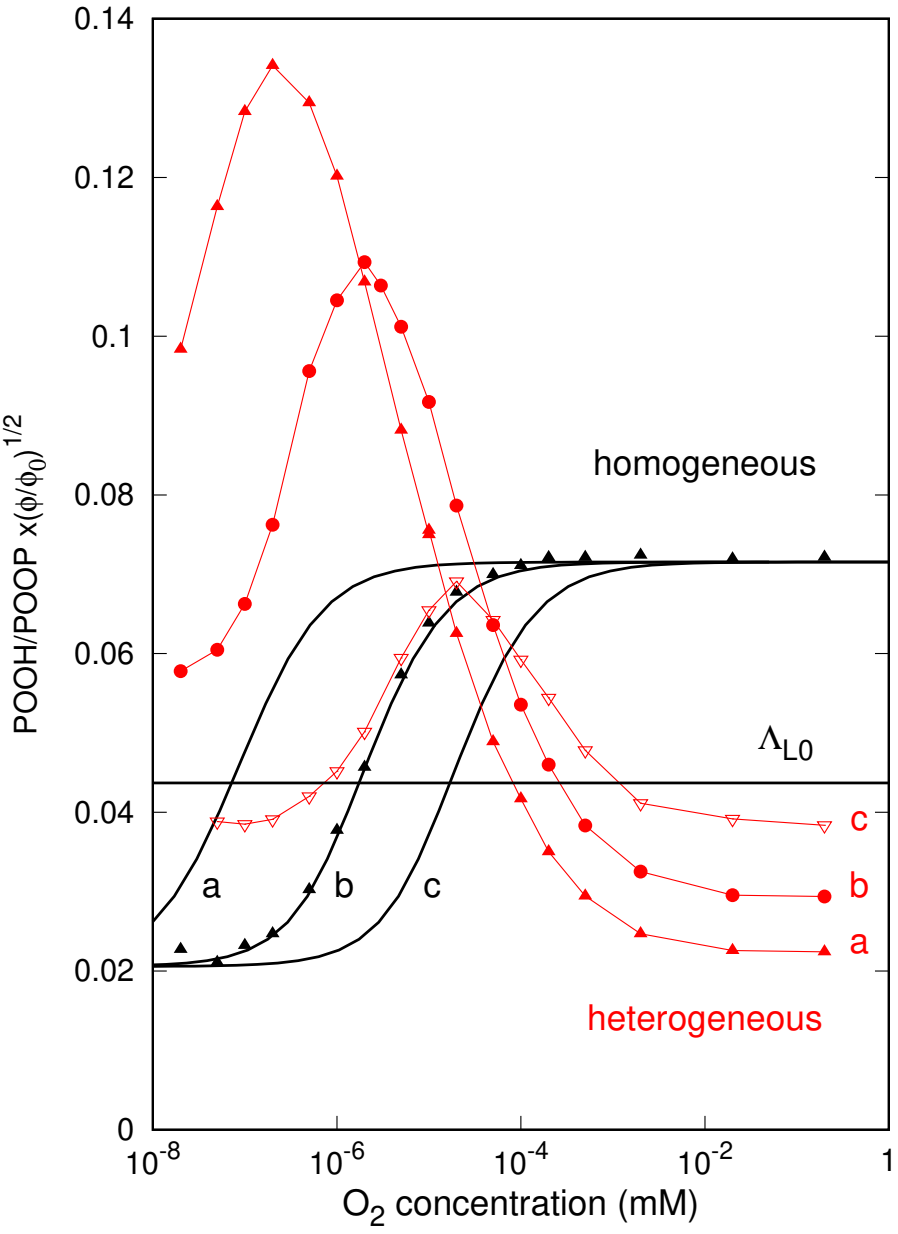

Figure 7: Normalized yield ratio $\Lambda\sqrt{\frac{\phi}{\phi_0}}$ for homogeneous and heterogeneous kinetics at three different dose rates: 6.1 10^{-4} (a), 6.1 (b) and 6.1 10^2 (c) kGy.h^{-1} corresponding respectively to flux ϕ equal to 10^3, 10^7 and 10^9 cm^{-2}s^{-1}. The reference flux is $\phi_0 = 10^7$ cm^{-2}s^{-1}. For the homogeneous case, the solid lines are numerical evaluations of the stationary yields (see section 2.3).